

Article

Impact of Partial Pressure, Conversion, and Temperature on the Oxidation Reaction Kinetics of Cu_2O to CuO in Thermochemical Energy Storage

Saman Setoodeh Jahromy ^{1,*}, Felix Birkelbach ², Christian Jordan ¹, Clemens Huber ¹, Michael Harasek ¹, Andreas Werner ² and Franz Winter ¹

¹ Institute of Chemical, Environmental and Bioscience Engineering, TU Wien, Getreidemarkt 9/166, 1060 Vienna, Austria; christian.jordan@tuwien.ac.at (C.J.); clemens.huber@tuwien.ac.at (C.H.); michael.harasek@tuwien.ac.at (M.H.); franz.winter@tuwien.ac.at (F.W.)

² Institute for Energy Systems and Thermodynamics, TU Wien, Getreidemarkt 9/302, 1060 Vienna, Austria; felix.birkelbach@tuwien.ac.at (F.B.); andreas.werner@tuwien.ac.at (A.W.)

* Correspondence: saman.setoodeh.jahromy@tuwien.ac.at

Received: 8 December 2018; Accepted: 1 February 2019; Published: 5 February 2019



Abstract: Metal oxides are promising potential candidates for thermochemical energy storage in concentrated solar power plants. In particular, the $\text{Cu}_2\text{O}/\text{CuO}$ system is suitable because of its high energy density, applied temperature interval, and reduced cost compared to the $\text{CoO}/\text{Co}_3\text{O}_4$ system. In heterogenous gas-solid reactions, the pressure affects the kinetics significantly. To quantify this effect for oxidation of Cu_2O to CuO , isothermal runs between 800 °C and 930 °C at different oxygen partial pressures (0.1, 0.2, 0.5, and 1.0 bar) were conducted with thermogravimetric analysis (TGA). Defined fractions of CuO samples (1–100 μm) were analyzed with X-ray diffraction (XRD), Brunauer-Emmett-Teller (BET) analysis, and scanning electron microscopy (SEM) analysis. The kinetic analyses were performed with extended non-parametric kinetics (NPK), which is applied for the first time to consider the pressure term in the general kinetic equation in addition to the conversion and the temperature term. The results show how the oxygen partial pressure impacts the kinetics and how reparameterization of the pressure term affects the kinetic analysis of the oxidation reaction of Cu_2O to CuO . The best conversion model is a two-dimensional Avrami-Erofeev model with an activation energy of 233 kJ/mol. The kinetic models for conversion, temperature, and pressure presented in this work provide one of the most important requirements for reactor designs.

Keywords: thermochemical energy storage; partial pressure; kinetics; thermogravimetric analysis; $\text{Cu}_2\text{O}/\text{CuO}$

1. Introduction

Humanity's demand for energy is increasing continuously due to population expansion and massive urbanization. According to the energy outlook of the International Energy Agency (IEA), fossil fuels will continue to contribute considerably to this energy demand [1], with the increase in CO_2 emissions impacting global warming. For instance, in the European Union (EU), around 40% of the CO_2 emissions are produced in the building sector by direct energy consumption [2]. To reduce CO_2 emissions, it is necessary to shift to renewable sources such as wind and solar energy, which are available everywhere and are relatively free of cost [3]. For this reason, concentrated solar power (CSP) has been developed to generate electricity from solar energy. Solar power plants can deliver energy whenever the sun is available, but the need for energy still exists especially in the winter season and during the night [4,5]. Therefore, the efficiency of CSP plants should be increased by storing the excess energy during sunny periods and the summer season. Here, "excess" expresses the

temporary overprovision of energy due to inelastic energy demand: The collected solar energy cannot be consumed when the energy is available. Therefore, it is essential to decouple energy production and consumption, for example, through the use of storage facilities [2].

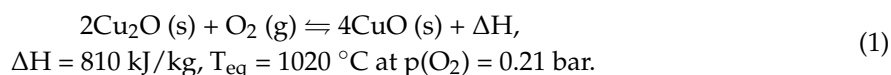
“Storing energy is a key challenge for the future for efficiency and sustainability of CSP plants” [6]. The surplus energy from CSP plants can be stored through water electrolysis by producing hydrogen gas and/or by methanation, which can be stored or injected into the gas grid [7–9]. This process, called power-to-gas (PtG), has been used worldwide and was reviewed by Götz et al. regarding the various technologies available and their advantages and drawbacks [10]. This storage process can be used by renewable sources, such as wind and solar energy. However, the efficiency of such conversion processes must be considered [11]. With the use of thermal energy storage, at least one of the conversion steps can be omitted (conversion from heat to electrical or mechanical energy).

Thermal energy storage is divided into sensible, latent, and thermochemical heat storage. Thermochemical energy storage is a promising concept due to its high energy density and zero energy loss [12–14]. Reversible reactions are used for the thermochemical energy storage system [15]. The exothermic reaction is used to release heat, and the endothermic (back) reaction is used to store heat. Thus, this system needs suitable materials for operation. Wang et al. investigated the use of sixteen different chemicals in CSP plants and suggested different metal oxides (Fe_2O_3 , BaO , Co_3O_4 , Mn_2O_3 , and CuO) suitable for thermochemical energy storage [16,17]. The equilibrium temperatures range from about $350\text{ }^\circ\text{C}$ to about $1100\text{ }^\circ\text{C}$, which means these metal oxides are suitable for improving the efficiency of CSP plants due to the high efficiency of CSPs at high operating temperatures [18,19].

Screening suitable materials at high temperature for thermochemical energy storage (TCES) has been the focus of many research groups [19–21]. Metal oxide systems are favored due to their high operating temperature ranges, high reaction enthalpies, longer storage periods at ambient temperature, and utilization of air not only as a reactant but also as a heat transfer medium [20–24]. Dizaji et al. and Wu et al. classified the redox metal oxides into two categories: Pure redox oxides and mixed redox systems [22,23]. They reviewed the advantages and disadvantages from various perspectives, such as energy density, reversibility of the reactions, kinetics, economics, and reactor types. In general, pure redox oxides have some drawbacks, such as low cycle stability, low kinetics, and sintering effects, which researchers have attempted to overcome by doping with other metal oxides [25–30].

The metal redox oxides $\text{Co}_3\text{O}_4/\text{CoO}$ and $\text{Cu}_2\text{O}/\text{CuO}$ have been investigated in recent research, because they possess the highest energy density, 844 and 810 kJ/kg, respectively. However, $\text{Cu}_2\text{O}/\text{CuO}$ have several unresolved challenges regarding application in TCES for this redox system, such as grain growth after thermal cycling, the close reduction temperature of CuO to the Cu_2O melting point of $1235\text{ }^\circ\text{C}$, and a decrease in the conversion rate with O_2 after the very low number of redox cycles reported by various authors [22,23,31–33]. However, the economic aspect and non-toxicity compared to $\text{Co}_3\text{O}_4/\text{CoO}$ make the redox system $\text{Cu}_2\text{O}/\text{CuO}$ interesting for utilization as a thermochemical energy storage material [6,33]. Figure 1 illustrates thermochemical energy storage for a $\text{Cu}_2\text{O}/\text{CuO}$ system. CuO is reduced to Cu_2O by an excess of thermal energy from CSP, and the stored energy in Cu_2O is released by an exothermic reaction with oxygen.

Equation (1) presents the reversible chemical reaction of $\text{Cu}_2\text{O}/\text{CuO}$ system with energy content and equilibrium temperature at oxygen partial pressure of 0.21 bar.



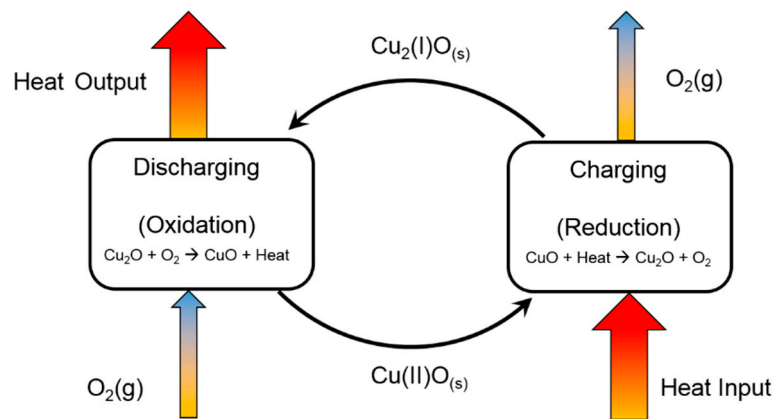


Figure 1. Thermochemical energy storage system for Cu₂O/CuO.

The kinetics of the Cu₂O/CuO system are essential for the reactor design and the operating parameters on a large scale [6]. CuO is used in the field of the chemical looping combustion as a copper-based oxygen carrier. Thus, various authors have reported investigating the kinetics of the reduction of CuO to Cu₂O and the oxidation of Cu₂O to CuO with different support materials, such as aluminum oxide, zirconium oxide, and titanium oxide [34–37]. Implementation of the those kinetics investigations in thermochemical energy storage would not be possible due to the impact of support materials on the kinetics of Cu₂O/CuO, which should be studied separately. In thermochemical energy storage, the kinetics of the reduction of CuO to Cu₂O was reported by Deutsch et al. [33] in simultaneous thermal analysis (STA) and in a fixed-bed reactor. They indicated cycle stability of Cu₂O/CuO system up to 20 cycles at 950 °C and at an oxygen partial pressure of 0.21 bar for the oxidation reactions, reduction was carried out in a nitrogen atmosphere. However, they did not study the impact of the oxygen partial pressure on the kinetics.

Therefore, to identify the impact of the oxygen partial pressure term on the general kinetic equation, which is usually neglected or is assumed to be constant at a constant oxygen partial pressure, this work investigates the oxidation reaction of Cu₂O to CuO. The reaction rate expression commonly consists of three terms: The temperature term $k(T)$, the reaction model $f(\alpha)$, and the pressure term $h(P)$. For $k(T)$, the Arrhenius equation is normally used in solid state reactions. The model term $f(\alpha)$ is different from reaction to reaction based on the different mechanism of each reaction. The equation below presents the general kinetic equation:

$$d\alpha/dt = k(T)f(\alpha)h(P) \quad (2)$$

To identify the pressure term $h(P)$ in a general kinetic equation, isothermal runs were performed at 930 °C, 870 °C, 830 °C, and 800 °C for oxygen partial pressure variations (0.1, 0.2, 0.5, and 1.0 bar) with STA. The mass signals resulting from the STA experiments were used to evaluate the conversions (α) based on the following equation:

$$\alpha = \frac{m_i - m(t)}{m_i - m_\infty} \quad (3)$$

where m_i is the initial mass, $m(t)$ is the mass at time t , and m_∞ is the mass at the end of the reaction. Non-parametric kinetics (NPK) was used to evaluate the kinetic data and the effect of the oxygen partial pressure on the oxidation kinetics of Cu₂O to CuO.

The NPK method is one of the more recent methods for modeling gas-solid reactions. It is based on the observation that the discretization of the general kinetic equation results in a rank-1 matrix, when only the $f(\alpha)$ and $k(T)$ terms are considered. To derive the kinetic model from experimental data, the values are arranged in a matrix, and rank-1 approximation methods are used to separate the contribution of each variable.

Model fitting can then be performed independently for each term of the general kinetic equation, which is generally easier and less prone to error than direct model fitting. The main advantage of the NPK method is that it can derive kinetic models from any combination of experiments without any additional a priori assumptions.

The NPK method was originally developed by Serra et al. [38–40] and later extended by various authors [41–44]. The method for evaluating the kinetics for this work is based on the NPK method extended by Birkelbach et al. [45]. This NPK method allows the derivation of kinetic models in more than two variables. With this method, we can also model the pressure dependence of the reaction.

2. Materials and Method

CuO from Merkur Emsure was sieved after grinding using a Retsch planetary ball mill PM 100. According to the investigation of Sahir et al. [46], the oxidation kinetics of copper is in the chemically controlled regimes, in particles ranging between 100 μm and 300 μm up to 800 $^{\circ}\text{C}$, while reactions of particles ranging in size from 800 μm to 1000 μm were affected by mass transfer. Therefore, the particles selected for this kinetic study ranged in size from 1 μm to 100 μm .

Following the recommendations of the International Confederation for Thermal Analysis and Calorimetry (ICTAC) [47,48], the sample mass of CuO for the STA experiments in this work was reduced significantly to minimize the transport effects on the kinetic measurements.

2.1. Particle Size Distribution (PSD)

A certain fraction after sieving was analyzed using a Mastersizer 2000 by Malvern Panalytical. A dispersion module with water as the dispersing fluid was used, and the measured interval was between 0.020 and 2000 μm .

2.2. X-ray Diffraction (XRD)

X-ray analysis was performed at the X-ray center at the TU Wien. A PANalytical X'Pert diffractometer (Panalytical, Malvern, UK) in Bragg-Brentano geometry was used. Radiation was generated by Cu $K\alpha_{1,2}$, and an X'Cleoraor linear detector with a Ni filter was in action. The sample was spun with back loading zero background sample holders and $2\theta = 5\text{--}90^{\circ}$ at 25 $^{\circ}\text{C}$. The diffractograms were evaluated with the PANalytical program suite HighScorePlus, version 3.0d. A Background correction and a $K\alpha_2$ strip were performed" [33].

2.3. Brunauer-Emmett-Teller (BET) Analysis

The physisorption measurement was executed by ASAP 2020 (Micromeritics GmbH, Aachen, Germany). To eliminate the adsorbed gases and moisture from the sample, the sample was heated up to 120 $^{\circ}\text{C}$ under vacuum for several hours.

2.4. Simultaneous Thermal Analysis

For the kinetic measurements, a Netzsch STA 449 Jupiter instrument (Erich Netzsch GmbH & Co. Holding KG, Germany) with a TGA-DSC sample holder were used. The oven temperature range of the instrument was between 25 $^{\circ}\text{C}$ and 1250 $^{\circ}\text{C}$, which was regulated by an S-Type thermocouple. The gas flow rates of oxygen and nitrogen were controlled using red-y smart Voegtlin. Aluminum oxide crucibles without lids were used for all experiments. The inert gas nitrogen with a flow rate of 100 ml/min was adjusted for each experimental run. Before each experiment was started, the sample in the reactor was flowed by nitrogen (99.999 % [v/v]) for a minimum of 30 min to remove oxygen from the reactor [47,48].

2.5. Scanning Electron Microscopy

The scanning electron microscopy (SEM) analysis was performed before and after the thermal treatment with FEI Quanta 200 FEG SEM (FEI, USA), which is equipped with a Schottky emitter in the operating range of 200 V to 30 KV with an Everhart-Thornley Detector for secondary electrons in action.

3. Results and Discussion

3.1. Material Analysis

The X-ray diffractometer indicated a purity of 99.8% for the CuO sample, and the BET analysis results for the CuO sample represented a surface area of $1.3 \text{ m}^2/\text{g}$. The PSD result in Figure 2 illustrates a bimodal distribution of CuO between 1 and $100 \text{ }\mu\text{m}$ with two local maxima at $5 \text{ }\mu\text{m}$ (7%) and $34 \text{ }\mu\text{m}$ (4%).

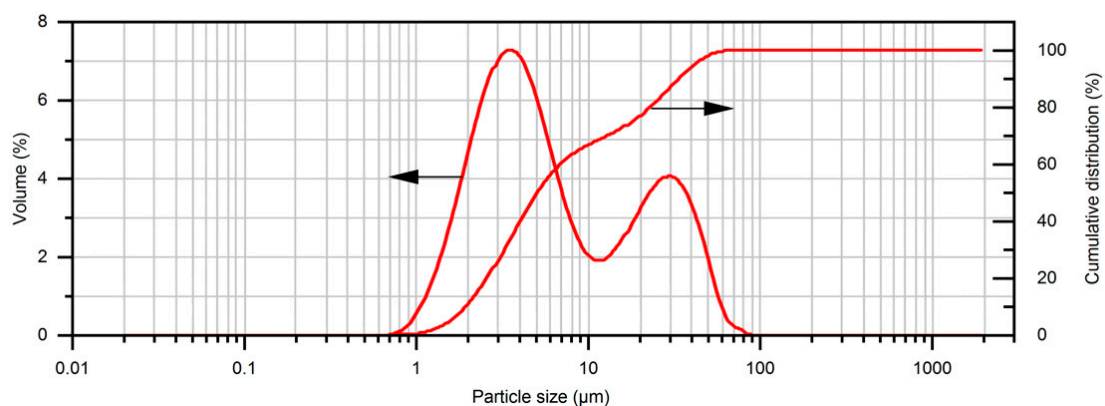


Figure 2. Particle size distribution of CuO.

3.2. Equilibrium Curve and Concept of Measurements

First, to prove whether the equilibrium oxygen pressure for the $\text{Cu}_2\text{O}/\text{CuO}$ system derived from the thermodynamic data from the HSC software [49] agrees with the experimental data, CuO was reduced under six different oxygen partial pressures (0.01, 0.3, 0.5, 0.1, 0.15, and 0.2 bar). In Figure 3, the points indicate the measured temperatures and pressures at which CuO was reduced to Cu_2O . The line is a generated equilibrium oxygen pressure curve from the thermodynamic data resulting from the HSC database [49]. As illustrated in Figure 3, the experimental data are in very good agreement with the theoretical data.

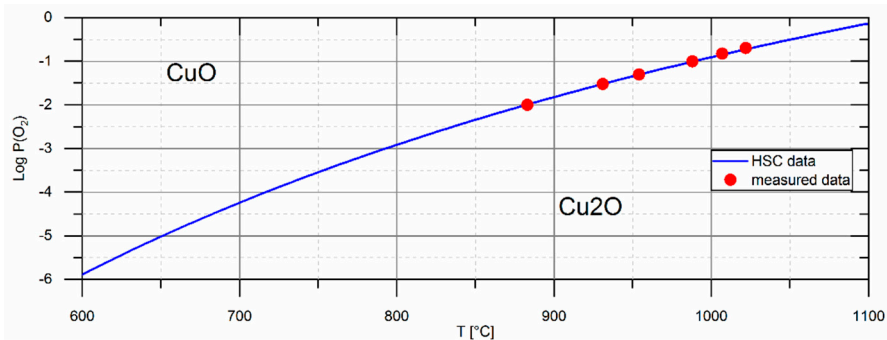


Figure 3. Comparison of the equilibrium oxygen pressure resulting from the HSC database [49] and the experimental data for $\text{Cu}_2\text{O}/\text{CuO}$.

Figure 4 shows all measured data at four temperature levels and four oxygen partial pressures at each temperature.

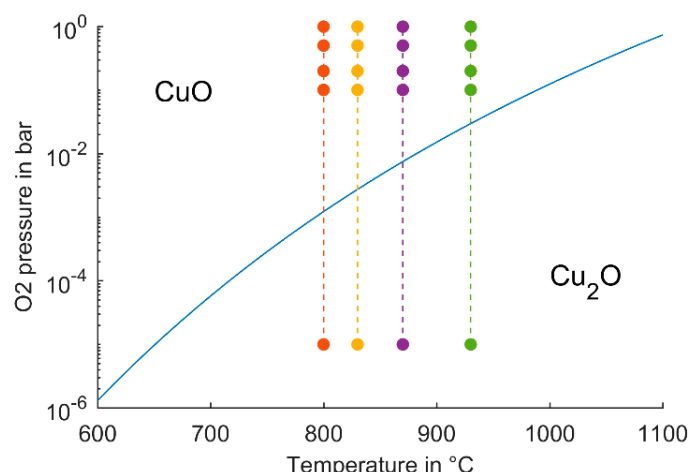


Figure 4. Representation of the operating conditions for the measurements relative to the equilibrium curve for the reaction system: Four temperature levels (800, 830, 870, 930 °C) and four partial oxygen partial pressures (0 bar for reduction, 0.1, 0.2, 0.5 and 1 bar for oxidation) at each temperature have been selected for the experiments.

Figure 5 illustrates an isothermal run for the oxidation of Cu_2O at 800 °C in the STA experiment. The mass signal is represented in green and the temperature profile as a dashed line in red.

The initial material was CuO and was reduced at higher temperatures to Cu_2O by decreasing the mass by 10.25%. The oxidation of Cu_2O to CuO was performed at oxygen partial pressures of 1.0, 0.5, 0.2, and 0.1 bar. At each temperature level, a new sample was used in the STA for four consecutive reduction/oxidation cycles. The conversions were between 94 and 100 wt%.

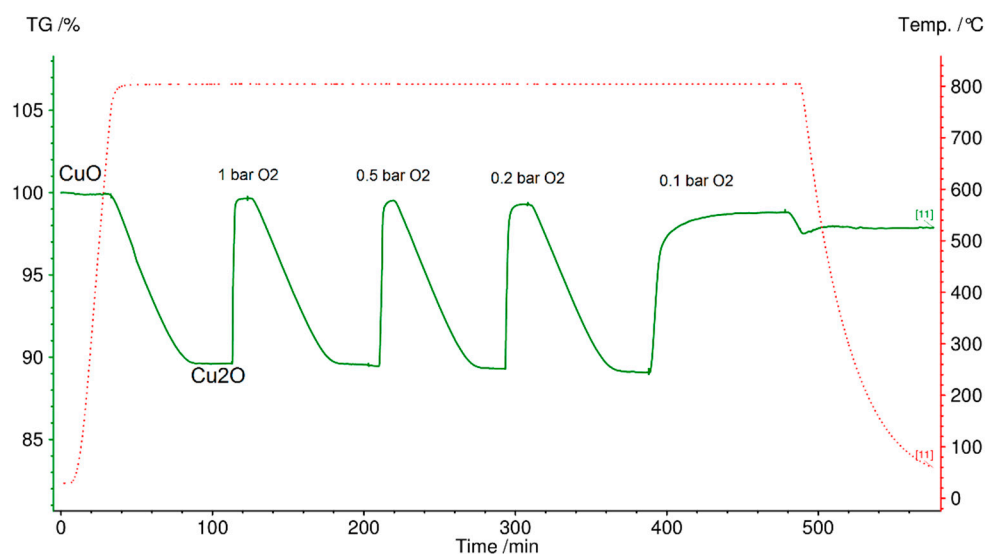


Figure 5. Experimental run for oxidation and reduction of Cu_2O and CuO , respectively, at 800 °C and different oxygen partial pressures in the simultaneous thermal analysis (STA).

Comparable results were also obtained at other temperatures, for example, 930 °C, once again with the same sample subjected to multiple oxidation/reduction steps. The differential scanning calorimetry (DSC) results are presented in Figure 6. The area indicates the relative reaction enthalpy for the reduction (endothermic, positive peaks) and the oxidation (exothermic, negative peaks), respectively. Using the energy calibration, the specific energy storage densities can be calculated, which are given in Table 1. It was found that despite the visible change (the DSC peak shape and magnitude in Figure 6) in the reaction rate with the oxygen partial pressure for the oxidation steps the

integrated peak area remained constant (within the experimental error) at about 1400–1650 μVs , which is equivalent to an energy storage density of approximately 510–600 kJ/kg of CuO. The peak areas for the reduction steps (always using N_2) resulted in 1450 μVs and 520 kJ/kg, respectively, which agrees reasonably well with the results for the oxidation reaction.

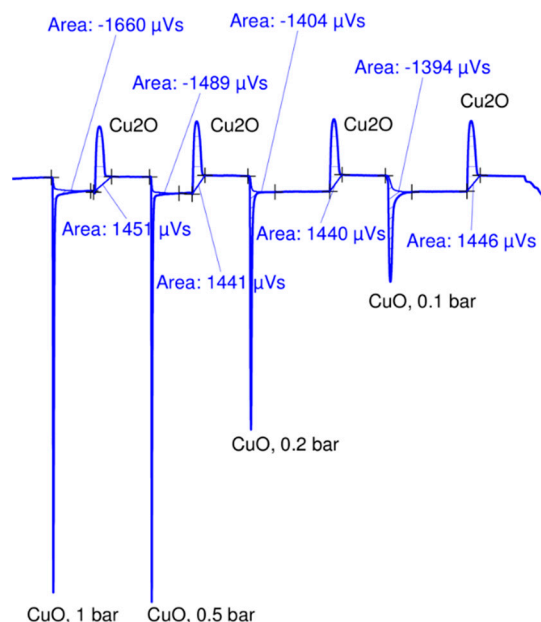


Figure 6. Differential scanning calorimetry (DSC) peaks of oxidation and reduction of $\text{Cu}_2\text{O}/\text{CuO}$ at 930 °C with variation in the partial pressures (1.0, 0.5, 0.2, and 0.1 bar).

Table 1. Specific energy content in kJ/kg of the reduction (charge) and oxidation (discharging) steps of the $\text{Cu}_2\text{O}/\text{CuO}$ system for each cycle at 930 °C.

Energy Content in kJ/kg	1. Cycle	2. Cycle	3. Cycle	4. Cycle
Charging (Reduction, N_2 atmosphere)	525	522	521	523
Discharging (Oxidation)	601	539	508	505
$p\text{O}_2$ (bar)	1.0	0.5	0.2	0.1

There is a significant deviation between theoretical (810 kJ/kg) and experimental (505–601 kJ/kg) specific energy content of the material, despite the up to 100 % conversion measured by TGA—this might result from using open TGA/DSC crucibles for the measurements (energy losses to gas stream). However, this does not influence the relative comparison of the values with regard to cycle stability and has also no effects on the kinetics evaluations.

3.3. Impact of Mass on Kinetic Measurements

To our knowledge, the impact of the sample mass on the kinetics of the $\text{Cu}_2\text{O}/\text{CuO}$ system has not been investigated. ICTAC [47,48] recommends 1 mg mass loss for kinetic studies, which means 10 mg in the case of copper oxide. However, to find the impact of the mass on the kinetic measurements, the conversion curve of four different masses (50.0, 10.0, 8.27, and 2.20 mg) was evaluated. Figure 7 illustrates the comparison of the conversions and the conversion rates vs. time for the oxidation of Cu_2O at an oxygen partial pressure of 0.1 bar and at 930 °C. It can be seen that the trend of the conversion curve of the sample with a mass of 50 mg is more influenced by the heat and mass transfer compared to the other masses. The conversion curve of the mass with 8.27 mg and 2.20 mg copper oxide shows a similar trend until the 0.8 conversion. Therefore, a mass of 8.29 ± 0.60 mg was selected for the kinetic study of this work. To minimize the temperature gradient, the sample was distributed

on the bottom of the crucible thus that the height of the sample for each experiment was several hundred micrometers [47,48].

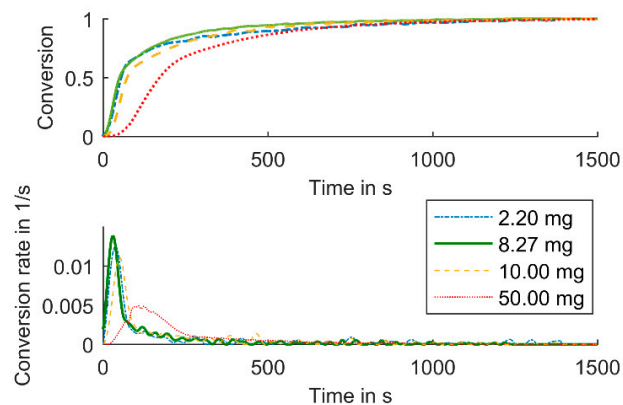


Figure 7. Impact of mass on conversions and conversion rates for oxidation of Cu_2O at a 0.1 bar oxygen partial pressure and at 930°C .

3.4. Evaluation of the Kinetics

Figure 8 illustrates the conversions and the conversion rates at the temperature levels 800°C and 830°C . It can be observed that the increase in the oxygen partial pressure increases the reaction rate and reduces the time required for full conversion. The same behavior of the impact of the pressure was observed at 870°C and 930°C . Figure 8 shows that a temperature increase of 30°C from 800°C to 830°C significantly impacts the conversion rate of the oxidation kinetics by a factor of five. This means that the same conversion of oxidation can be reached around five times faster at 830°C than at 800°C at the same partial pressure. Therefore, the time axis in Figure 8 has been adjusted accordingly.

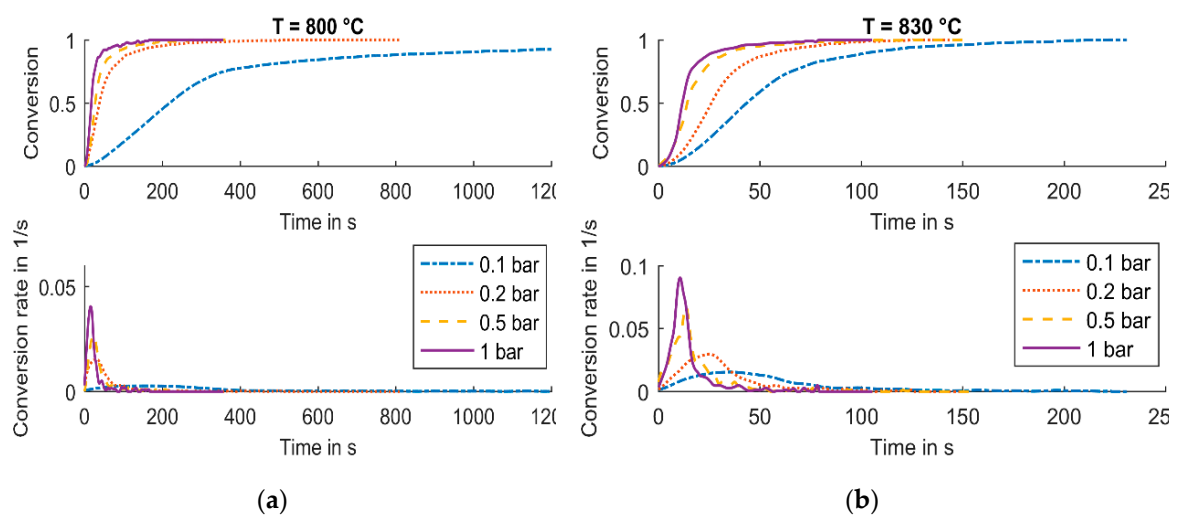


Figure 8. Influence of different oxygen partial pressures on reactions and reaction rates at two temperatures, 800°C and 830°C . Please note the different time axes for 800°C (a) and 830°C (b).

Figure 9 shows all measurements in a diagram with conversion, temperature, and pressure axes. Figure 9 illustrates the conversion at four temperature levels and four pressure levels of all measured data. The colors are related to the conversion rates. The brighter the color, the higher the reaction rates.

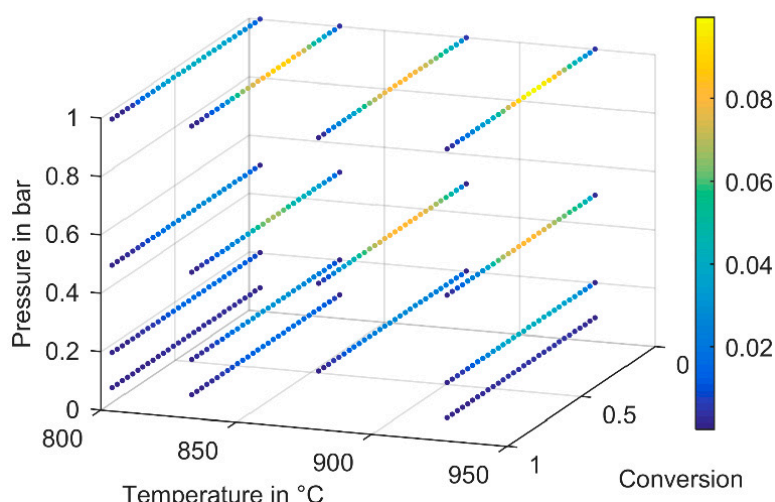


Figure 9. All measured data in conversion, temperature, and pressure (ctp) diagram.

Figure 10 shows the conversion term and the pressure term at each experimented temperature level. The points are the experimental data with error bars, which relate to the standard deviation. Due to the non-prior model estimation by NPK, the trend of each model determined should be fitted to the known models (nucleation, diffusion, order-based, and geometric contraction models). Some models are represented in Table 2.

The best fitted models with the largest regression coefficient are the A2 and A5 models. Avrami-Erofeev (A2, A3, A4, and A5) models are nucleation models with different nucleation types and crystal dimensionality [50,51]. Nucleation models are normally used to describe many solid-state reactions, such as crystallization crystallographic transition, decomposition, adsorption, hydration, and desolvation [50–63]. Due to the existence of impurities, cracks, edges, dislocations, and defect points in each of the crystals, the activation energy is minimized on these sites [54,61,62]. These reactive sites are called nucleation sites [54,61,62], which attain high reactivity, and on these sites, a new phase (CuO) can start to form in the lattice of Cu₂O.

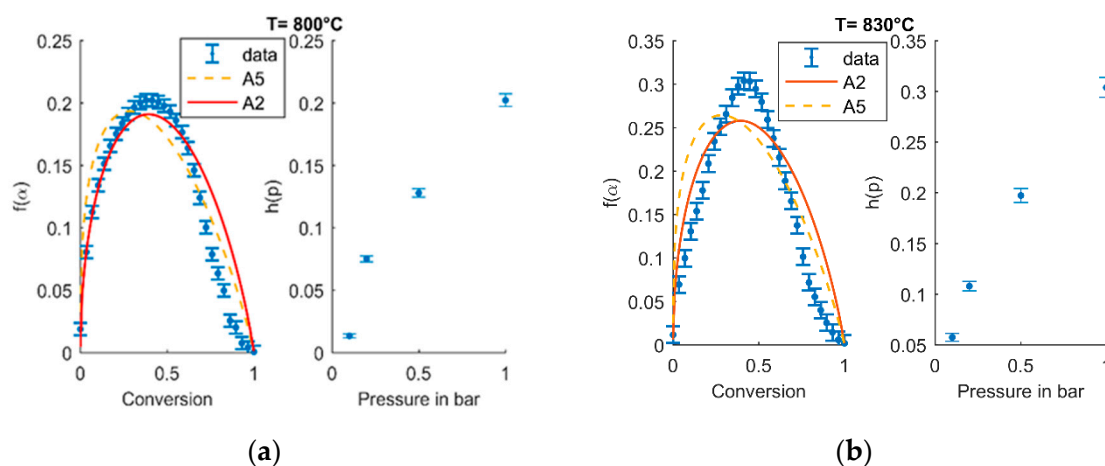


Figure 10. Best fitted models (A2 = continuous red line, A5 = yellow dashed line) to the experimental data and the impact of the pressure on the kinetics by non-parametric kinetics (NPK) at 800 °C (a) and at 830 °C (b).

Table 2. Some models of solid-state reactions for conversion dependence [48,60,61].

Model ID	Type	$f(\alpha)$
A1	Avrami-Erofeev	$4(1-\alpha)[-ln(1-\alpha)]^{3/4}$
A2	Avrami-Erofeev	$2(1-\alpha)[-ln(1-\alpha)]^{1/2}$
A3	Avrami-Erofeev	$3(1-\alpha)[-ln(1-\alpha)]^{2/3}$
A4	Avrami-Erofeev	$4(1-\alpha)[-ln(1-\alpha)]^{3/4}$
A5	Avrami-Erofeev	$3/2(1-\alpha)[-ln(1-\alpha)]^{1/3}$
B1	Prout-Tompkins	$\alpha(1-\alpha)$
R2	Contracting area	$2(1-\alpha)^{1/2}$
R3	Contracting volume	$3(1-\alpha)^{2/3}$
R4	Interface	$3/2(1-\alpha)^{1/3}$
D1	1-D diffusion	$1/(2\alpha)$
D2	2-D diffusion	$-[1/ln(1-\alpha)]$
D3	3-D diffusion-Jander	$[3(1-\alpha)^{2/3}]/[2(1-(1-\alpha)^{1/3})]$
F0/R1	Zero-order	1
F1	First-order	$(1-\alpha)$
F2	Second-order	$(1-\alpha)^2$
F3	Third-order	$(1-\alpha)^3$

Two-dimensional nucleation according to the Avrami-Erofeev model (A2) showed a better fit than the other nucleation models. The pressure trend is also illustrated in Figure 11, which proves that an increase in the oxygen partial pressure leads to an increase in the pressure term in the general kinetic equation.

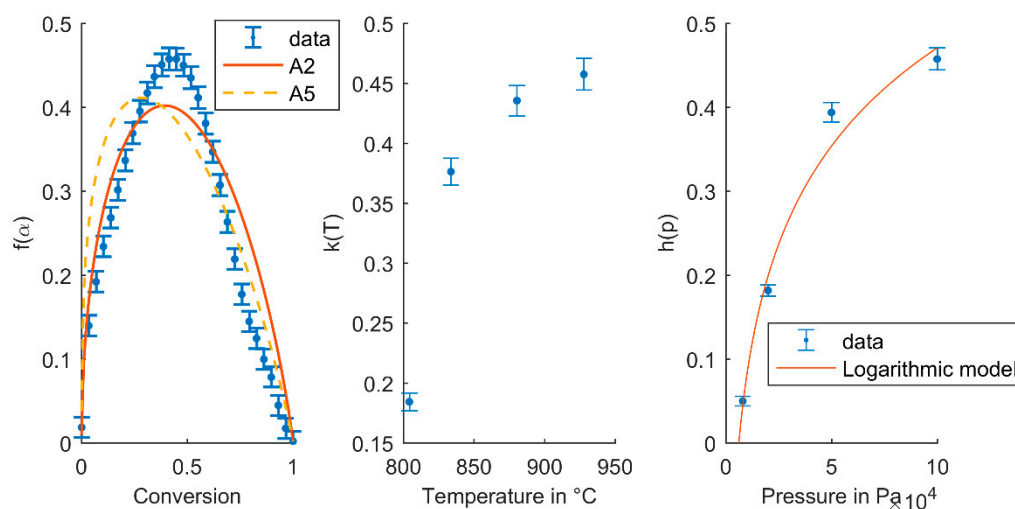


Figure 11. Model generated from all data measured with the NPK method and the best models fitted (A2 and A5) to the experimental data, temperature, and pressure dependences.

Figure 11 exhibits the model term, temperature term, and pressure term by considering all kinetic data presented by using the NPK method. The A2 model is the best fitted model with the highest regression coefficient ($R^2 = 0.89$) and an activation energy of 76.7 kJ/mol. It can be seen that the model and pressure trends are the same as the previously evaluated models and pressures at each temperature level (see Figure 11). However, the temperature trend does not match the exponential trend of the Arrhenius equation. Unusual Arrhenius trends at high temperatures were observed and reported by Kyaw et al. [64] in their study “Carbonation of CaO for High Temperature Thermal Energy Storage” and by Schaube et al. [65] for the CaO/Ca(OH)₂ system at high H₂O partial pressures. Deutsch et al. found a negative activation energy for the CuO/Cu₂O system in STA experiments [33].

Distance to the equilibrium was not considered for the kinetic evaluation presented above. To consider the pressure influence on the kinetic evaluation, the pressure parameter was reparameterized to $(1-P/P^*)^n$ for considering the distance of the equilibrium curve in the general kinetic equation. The result of this reparameterization (Figure 12) shows close temperature dependence to the weighted Arrhenius equation. The pressure term indicates the distance to the equilibrium oxygen partial pressure and consequently, its impact on the kinetics. The influence of the pressure term on the kinetics decreases if the oxygen partial pressure P , adjusted for the reaction, is close to the equilibrium oxygen partial pressure P^* (Sections 3 and 3.2; see Figure 3), which moves the Equation (1) $-P/P^*$ toward zero.

After reparameterization, the model stays the same (A2) with a regression coefficient of $R^2 = 0.87$, an activation energy of 233 kJ/mol, and a frequency factor of 5×10^9 1/s. The general kinetic equation for the oxidation kinetics of Cu_2O to CuO in the temperature range between 800 °C and 930 °C by variation in the oxygen partial pressures (0.1, 0.2, 0.5, and 1.0 bar) can be written as follows:

$$d\alpha/dt = 5 \times 10^9 \times e^{(-233000/RT)} \times 2(1-\alpha)[- \ln(1-\alpha)]^{1/2} \times a(1-P/P^*)^{0.658}. \quad (4)$$

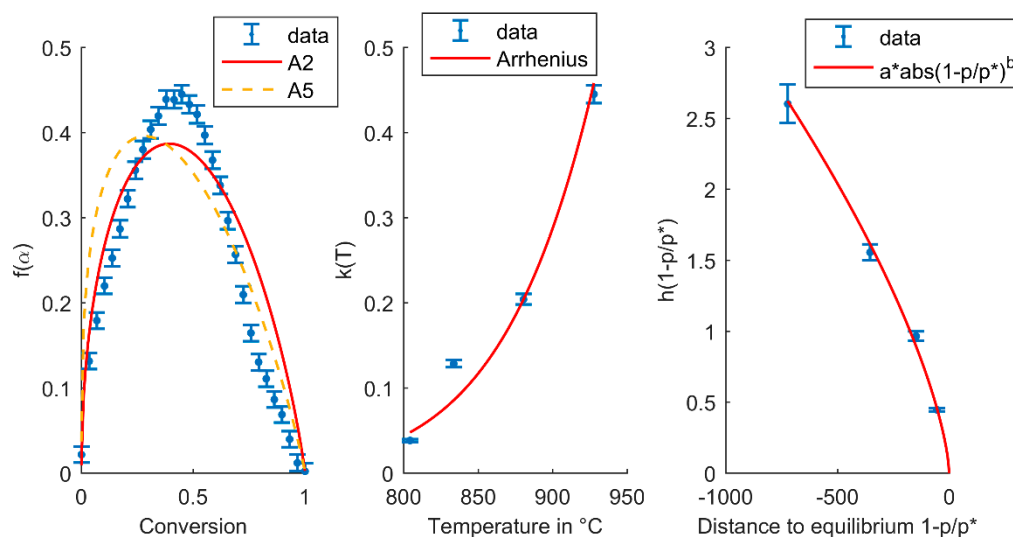


Figure 12. Reparameterization of pressure for considering the distance to the equilibrium curve in the general kinetic equation.

The trend of the conversion model of the experimental data in all kinetic evaluations indicated different behavior from the Avrami-Erofeev models at the end of the reactions ($\alpha = 0.7-0.8$), which led to a reduction in the model regression coefficient. This observation could be the result of changing the mechanism of the reaction at the end of Cu_2O oxidation, due to the formation of the CuO layer around the Cu_2O core [66,67] that leads to limitations in oxygen transfer to the reactive Cu_2O . However, this issue should be studied separately.

4. Scanning Electron Microscopy

Figure 13 shows the CuO particles before and after the experimental run by STA. Pure CuO particles are visible, but after the STA runs, the particles do not exist due to agglomeration and the sintering effect, which created an area of CuO with cavities. The sintering effect of CuO is a disadvantage, which results in material aging and a negative impact on cycle stability in the long term. The same results were reported by Deutsch et al. [33] in a fixed-bed reactor and STA, but Alonso et al. reported better results in a rotary kiln [6].

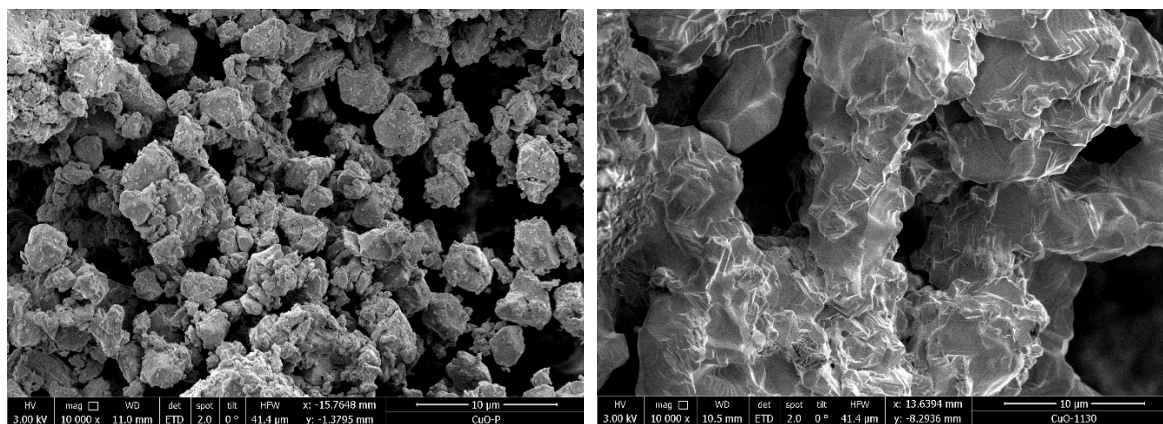


Figure 13. Comparison of the particle change of CuO before (left) and after (right) the simultaneous thermal analysis (STA) experiment.

5. Conclusions

The investigation of the effect of the sample mass on the oxidation kinetics of Cu_2O to CuO shows that a sample mass of less than 10 mg is required for the kinetic analyses to minimize the transport effects on the kinetic measurements.

The equilibrium oxygen pressure for the $\text{Cu}_2\text{O}/\text{CuO}$ system was tested experimentally, and the results are in very good agreement with the theoretical equilibrium oxygen pressure generated by the HSC software [49].

The extended NPK method [45] was used for the first time for this application, which determines the pressure, conversion, and temperature terms of the oxidation reaction of Cu_2O to CuO for its utilization in thermochemical energy storage. The best conversion model was Avrami-Erofeev's two-dimensional nucleation model (A2) with an activation energy of 233 kJ/mol, and a frequency factor of 5×10^9 1/s. The reparameterization of the pressure term from P to $(1 - P/P^*)^n$ is essential to take into account the distance from equilibrium in the general kinetic equation.

Author Contributions: Conceptualization, S.S.J.; Data curation, S.S.J.; Formal analysis, S.S.J., F.B. and C.H.; Investigation, S.S.J., F.B. and C.J.; Methodology, F.B. and C.H.; Project administration, M.H. and A.W.; Resources, C.J., M.H., A.W. and F.W.; Software, F.B. and C.H.; Supervision, M.H., A.W. and F.W.; Validation, S.S.J., F.B. and C.J.; Visualization, S.S.J. and F.B.; Writing—original draft, S.S.J., F.B. and Franz Winter; Writing—review & editing, S.S.J., F.B., C.J., C.H. and F.W.

Funding: Austrian Research Promotion Agency (FFG), SolidHeat Pressure (#853593), SolidHeat Kinetics (#848876).

Acknowledgments: The authors thank the Austrian Research Promotion Agency (FFG) for the financial support of the project SolidHeat Pressure (853593) and SolidHeat Kinetics (848876). The X-ray center (XRC) and Universitäre Service-Einrichtung für Transmissions Elektronenmikroskopie (USTEM) of TU Wien are acknowledged for providing access to the powder X-ray diffractometers and scanning electron microscopy (SEM). Last but not least many thanks to the research group of Mechanical Engineering and Clean Air Technology of the institute for providing the Mastersizer 2000 for measuring the particle size distribution of samples. The authors acknowledge the TU Wien University Library for financial support through its Open Access Funding Program.

Conflicts of Interest: The authors declare no conflict of interest.

References

1. International Energy Agency (IEA). *World Energy Outlook*; IEA: Paris, France, 2017.
2. Tronchin, L.; Manfren, M.; Nastasi, B. Energy efficiency, side management and energy storage technologies—A critical analysis of possible paths of integration in the built environment. *Renew. Sustain. Energy Rev.* **2018**, *95*, 341–353. [[CrossRef](#)]
3. Alonso, E.; Gallo, A.; Perez-Rabago, C.; Fuentealba, E. Thermodynamic study of $\text{CuO}/\text{Cu}_2\text{O}$ and $\text{Co}_3\text{O}_4/\text{CoO}$ redox pairs for solar energy thermochemical storage. *AIP Conf. Proc.* **2016**, *1734*, 050004.

4. Romero, M.; Steinfeld, A. Concentrating solar thermal power and thermochemical fuels. *Energy Environ. Sci.* **2012**, *5*, 9137–9674. [[CrossRef](#)]
5. Zaversky, F.; Garcia-Barberena, J.; Sanchez, M.; Astrain, D. Transient molten salt two-tank thermal storage modeling for CSP performance simulations. *Sol. Energy* **2013**, *93*, 294–311. [[CrossRef](#)]
6. Alonso, E.; Perez-Rabago, C.; Licurgo, J.; Fuentealba, E.; Estrada, A.C. First experimental studies of solar redox reactions of copper oxides for thermochemical energy storage. *Sol. Energy* **2015**, *115*, 297–305. [[CrossRef](#)]
7. Miltner, M.; Makaruk, A.; Harasek, M. Investigation of the long-term performance of an industrial-scale biogas upgrading plant with grid supply applying gas permeation membranes. *Chem. Eng. Trans.* **2010**, *21*, 1213–1218. [[CrossRef](#)]
8. Liemberger, W.; Halmschlager, D.; Miltner, M.; Harasek, M. Efficient extraction of hydrogen transported as co-stream in the natural gas grid—The importance of process design. *Appl. Energy* **2019**, *233–234*, 747–763. [[CrossRef](#)]
9. Biegger, P.; Kirchbacher, F.; Medved, A.R.; Miltner, M.; Lehner, M.; Harasek, M. Development of honeycomb methanation catalyst and its application in power to gas systems. *Energies* **2018**, *11*, 1679. [[CrossRef](#)]
10. Götz, M.; Lefebvre, J.; Mörs, F.; McDaniel Koch, A.; Graf, F.; Bajohr, S.; Reimert, R.; Kolb, T. Renewable Power-to-Gas: A technological and economic review. *Renew. Energy* **2016**, *85*, 1371–1390. [[CrossRef](#)]
11. Kirchbacher, F.; Biegger, P.; Miltner, M.; Lehner, M.; Harasek, M. A new methanation and membrane based power-to-gas process for the direct integration of raw biogas—Feasibility and comparison. *Energy* **2018**, *146*, 34–46. [[CrossRef](#)]
12. Aydin, A.; Casey, P.S.; Riffat, S. The latest advancements on thermochemical heat storage systems. *Renew. Sustain. Energy Rev.* **2015**, *41*, 356–367. [[CrossRef](#)]
13. Agrafiotis, C.; Roeb, M.; Sattler, C. Hybrid sensible/thermochemical solar energy storage concepts based on porous ceramic structures and redox pair oxides chemistry. *Energy Procedia* **2015**, *69*, 706–715. [[CrossRef](#)]
14. Abedin, A.H.; Rosen, M.A. A critical review of thermochemical energy storage systems. *Open Renew. Energy J.* **2011**, *4*, 42–46. [[CrossRef](#)]
15. Dai, L.; Long, X.; Lou, B.; Zhou, S.; Xu, Y. Progress in thermochemical energy storage for concentrated solar power: A review. *Int. J. Energy Res.* **2018**, *42*, 4546–4561.
16. Wong, B. *Thermochemical Heat Storage for Concentrated Solar Power: Thermochemical System Reactor Design for Thermal Energy Storage: Phase II Final Report for the Period September 30, 2008 through April 30, 2011*; U.S. Department of Energy: Washington, DC, USA, 2011.
17. Wong, B.; Brown, L.; Schaube, F.; Tamme, R.; Sattler, C. Oxide based thermochemical heat storage. In Proceedings of the 16th Solar PACES Conference, Perpignan, France, 21–24 September 2010.
18. Stekli, J.; Irwin, L.; Pitchumani, R. Technical challenges and opportunities for concentrating solar power with thermal energy storage. *J. Thermal Sci. Eng. Appl.* **2013**, *5*, 021011. [[CrossRef](#)]
19. Pardo, P.; Deydier, A.; Anxionnaz-Minvielle, Z.; Rouge, S.; Cabassud, M.; Cognet, P. A review on high temperature thermochemical heat energy storage. *Renew. Sustain. Energy Rev.* **2014**, *32*, 591–610. [[CrossRef](#)]
20. Andre, L.; Abanades, S.; Flamant, G. Screening of thermochemical systems based on solid-gas reversible reactions for high temperature solar thermal energy storage. *Renew. Sustain. Energy Rev.* **2016**, *64*, 703–715. [[CrossRef](#)]
21. Deutsch, M.; Müller, D.; Aumeyr, C.; Jordan, C.; Gierlmayer, C.; Weinberger, P.; Winter, F.; Werner, A. Systematic search for potential thermochemical energy storage systems. *Appl. Energy* **2016**, *183*, 113–120. [[CrossRef](#)]
22. Beidaghy Dizaji, H.; Hosseini, H. A review of material screening in pure and mixed-metal oxide thermochemical energy storage (TCES) systems for concentrated solar power (CSP) applications. *Renew. Sustain. Energy Rev.* **2018**, *98*, 9–26. [[CrossRef](#)]
23. Wu, S.; Zhou, C.; Doroodchi, E.; Nellore, R.; Moghtaderi, B. A review on high-temperature thermochemical energy storage based on metal oxides redox cycle. *Energy Convers. Manag.* **2018**, *168*, 421–453. [[CrossRef](#)]
24. Agrafiotis, C.; Roeb, M.; Schmücker, M.; Sattler, C. Exploitation of thermochemical cycles based on solid oxide redox systems for thermochemical storage of solar heat. Part 1: Testing of cobalt oxide-based powders. *Sol. Energy* **2014**, *102*, 189–211. [[CrossRef](#)]

25. Agrafiotis, C.; Roeb, M.; Sattler, C. Exploitation of thermochemical cycles based on solid oxide redox systems for thermochemical storage of solar heat. Part 4: Screening of oxides for use in cascaded thermochemical storage concepts. *Sol. Energy* **2016**, *139*, 695–710. [[CrossRef](#)]
26. Block, T.; Knoblauch, N.; Schmücker, M. The cobalt-oxide/iron-oxide binary system for use as high temperature thermochemical energy storage material. *Thermochim. Acta* **2014**, *577*, 25–32. [[CrossRef](#)]
27. Block, T.; Schmücker, M. Metal oxides for thermochemical energy storage: A comparison of several metal oxide systems. *Sol. Energy* **2016**, *126*, 195–207. [[CrossRef](#)]
28. Carrillo, A.J.; Moya, J.; Bayon, A.; Jana, P.; de la Pena O Shea, V.A.; Romero, M.; Gonzalez-Aguilar, J.; Serrano, D.P.; Pizarro, P.; Coronado, J.M. Thermochemical energy storage at high temperature via redox cycles of Mn and Co oxides: Pure oxides versus mixed ones. *Sol. Energy Mater. Sol. Cells* **2014**, *123*, 47–57. [[CrossRef](#)]
29. Carrillo, A.F.; Serrano, D.P.; Pizarro, P.; Coronado, J.M. Improving the thermochemical energy storage performance of the Mn_2O_3/Mn_3O_4 redox couple by the incorporation of iron. *ChemSusChem* **2015**, *8*, 1947–1954. [[CrossRef](#)]
30. Andre, L.; Abanades, S.; Cassayre, L. Mixed metal oxide systems applied to thermochemical storage of solar energy: Benefits of secondary metal addition in Co and Mn oxides and contribution of thermodynamics. *Appl. Sci.* **2018**, *8*, 2618. [[CrossRef](#)]
31. Agrafiotis, C.; Becker, A.; Roeb, M.; Sattler, C. Hybrid sensible/thermochemical storage of solar energy in cascades of redox-oxide-pair-based porous ceramics. In Proceedings of the ASME 2015 9th International Conference on Energy Sustainability Collocated with ASME 2015 Power Conference, the ASME 2015 13th International Conference on Fuel Cell Science, Engineering and Technology, and the ASME 2015 Nuclear Forum, San Diego, CA, USA, 28 June–2 July 2015.
32. Chadda, D.; Ford, J.D.; Fahim, M.A. Chemical energy storage by the reaction cycle CuO/Cu_2O . *Int. J. Energy Res.* **1989**, *13*, 63–73. [[CrossRef](#)]
33. Deutsch, M.; Horvath, F.; Knoll, C.; Lager, D.; Gierl-Mayer, C.; Weinberger, P.; Winter, F. High-temperature energy storage: Kinetic investigations of the CuO/Cu_2O reaction cycle. *Energy Fuels* **2017**, *31*, 2324–2334. [[CrossRef](#)]
34. Clayton, K.C.; Sohn, H.Y.; Whitty, K.J. Oxidation kinetics of Cu_2O in oxygen carriers for chemical looping with oxygen uncoupling. *Ind. Eng. Chem. Res.* **2014**, *53*, 2976–2986. [[CrossRef](#)]
35. Clayton, C.K.; Whitty, K.J. Measurement and modeling of decomposition kinetics for copper oxide-based chemical looping with oxygen uncoupling. *Appl. Energy* **2016**, *116*, 416–423. [[CrossRef](#)]
36. Hu, W.; Donat, F.; Scott, S.A.; Dennis, J.S. Kinetics of oxygen uncoupling of a copper based oxygen carrier. *Appl. Energy* **2016**, *161*, 92–100. [[CrossRef](#)]
37. Adanez-Rubio, I.; Gayan, P.; Abad, A.; Garcia-Labiano, F.; de Diego, L.F.; Adanez, J. Kinetic analysis of a Cu-based oxygen carrier: Relevance of temperature and oxygen partial pressure on reduction and oxidation reactions rates in chemical looping with oxygen uncoupling (CLOU). *Chem. Eng. J.* **2014**, *256*, 69–84. [[CrossRef](#)]
38. Serra, R.; Nomen, R.; Sempere, J. The non-parametric kinetics a new method for the kinetic study of thermoanalytical data. *J. Thermal Anal. Calorim.* **1998**, *52*, 933–943. [[CrossRef](#)]
39. Serra, R.; Sempere, J.; Nomen, R. A new method for the kinetic study of thermoanalytical data: The non-parametric kinetics method. *Thermochim. Acta* **1998**, *316*, 37–45. [[CrossRef](#)]
40. Sempere, J.; Nomen, R.; Serra, R.; Soravilla, J. The NPK method—An innovative approach for kinetic analysis of data from thermal analysis and calorimetry. *Thermochim. Acta* **2002**, *388*, 407–414. [[CrossRef](#)]
41. Heal, G.R. A generalisation of the non-parametric, NPK (SVD) kinetic analysis method: Part 1. Isothermal experiments. *Thermochim. Acta* **2005**, *426*, 15–21. [[CrossRef](#)]
42. Heal, G.R. A generalisation of the non-parametric, NPK (SVD) kinetic analysis method: Part 2. Non-isothermal experiments. *Thermochim. Acta* **2005**, *426*, 23–31. [[CrossRef](#)]
43. Deutsch, M.; Birkelbach, F.; Knoll, C.; Harasek, M.; Werner, A.; Winter, F. An extension of the NPK method to include the pressure dependency of solid state reactions. *Thermochim. Acta* **2017**, *654*, 168–178. [[CrossRef](#)]
44. Birkelbach, F.; Deutsch, M.; Stylianos, F.; Winter, F.; Werner, A. A higher-order generalization of the NPK-method. *Thermochim. Acta* **2018**, *661*, 27–33. [[CrossRef](#)]
45. Birkelbach, F.; Deutsch, M.; Stylianos, F.; Winter, F.; Werner, F. NPK 2.0: Introducing tensor decompositions to the kinetic analysis of solid state reactions. *Int. J. Chem. Kinet.* **2019**, 1–11. [[CrossRef](#)]

46. Sahir, A.H.; Lighty, J.S. Kinetics of copper oxidation in the air reactor of a chemical looping combustion system using the law of additive reaction times. *Ind. Eng. Chem. Res.* **2011**, *50*, 13330–13339. [[CrossRef](#)]
47. Vyazovkin, S.; Burnham, A.K.; Criado, J.M.; Perez-Maqueda, L.A.; Popescu, C.; Sbirrazzuoli, N. ICTAC kinetics committee recommendations for performing kinetic computations on thermal analysis data. *Thermochim. Acta* **2011**, *520*, 1–19. [[CrossRef](#)]
48. Vyazovkin, S.; Chrissafis, K.; Di Lorenzo, M.L.; Koga, N.; Pijolat, M.; Roduit, B.; Sbirrazzuoli, N.; Sunol, J.J. ICTAC kinetics committee recommendations for collecting experimental thermal analysis data for kinetic computations. *Thermochim. Acta* **2014**, *590*, 1–23. [[CrossRef](#)]
49. Roine, A. *HSC Chemistry 6.12*; Outotec Research Oy: Pori, Finland, 2007.
50. Yang, J.; McCoy, B.J.; Madras, G. Kinetics of nonisothermal polymer crystallization. *J. Phys. Chem. B* **2005**, *109*, 18550–18557. [[CrossRef](#)] [[PubMed](#)]
51. Hay, J.N. Application of the modified avrami equations to polymer crystallisation kinetics. *Br. Polym. J.* **1971**, *3*, 74–82. [[CrossRef](#)]
52. Yang, J.; McCoy, B.J.; Madras, G. Cluster kinetics and dynamics during spinodal decomposition. *J. Phys. Chem.* **2006**, *124*, 024713. [[CrossRef](#)]
53. Liu, J.; Wang, J.; Li, H.; Shen, D.; Zhang, J.; Ozaki, Y.; Yan, S. Epitaxial crystallization of isotactic poly(methyl methacrylate) on highly oriented polyethylene. *J. Phys. Chem. B* **2006**, *110*, 738–742. [[CrossRef](#)]
54. Burnham, A.K.; Weese, R.K.; Weeks, B.L. A distributed activation energy model of thermodynamically inhibited nucleation and growth reaction and its application to the β - δ phase transition of HMX. *J. Phys. Chem. B* **2004**, *108*, 19432–19441. [[CrossRef](#)]
55. Graetz, J.; Reilly, J.J. Decomposition kinetics of AlH_3 polymorphs. *J. Phys. Chem. B* **2005**, *109*, 22181–22185. [[CrossRef](#)]
56. Wang, S.; Gao, Q.; Wang, J. Thermodynamic analysis of decomposition of thiourea and thiourea oxides. *J. Phys. Chem. B* **2005**, *109*, 17281–17289. [[CrossRef](#)]
57. Hromadova, M.; Sokolova, R.; Pospisil, L.; Fanelli, N. Surface interactions of s-Triazine-Type pesticides. An electrochemical impedance study. *J. Phys. Chem. B* **2006**, *110*, 4869–4874. [[CrossRef](#)] [[PubMed](#)]
58. Wu, C.; Wang, P.; Yao, X.; Liu, C.; Chen, D.; Lu, G.Q.; Cheng, H. Effects of SWNT and metallic catalyst on hydrogen absorption/desorption performance of MgH_2 . *J. Phys. Chem. B* **2005**, *109*, 22217–22221. [[CrossRef](#)] [[PubMed](#)]
59. Peterson, V.K.; Neumann, D.A.; Livingston, R.A. Hydration of tricalcium and dicalcium silicate mixtures studied using quasielastic neutron scattering. *J. Phys. Chem. B* **2005**, *109*, 14449–14453. [[CrossRef](#)] [[PubMed](#)]
60. Khawam, A. Application of Solid-State Kinetic to Desolvation Reactions. Ph.D. Thesis, University of Iowa, Iowa City, IA, USA, 2007.
61. Khawam, A.; Flanagan, D.R. Solid-State kinetic models: Basics and mathematical fundamentals. *J. Phys. Chem. B* **2006**, *110*, 17315–17328. [[CrossRef](#)] [[PubMed](#)]
62. Boldyrev, V.V. Topochemistry of thermal decompositions of solids. *Thermochim. Acta* **1986**, *100*, 315–338. [[CrossRef](#)]
63. Jacobs, P.W.M.; Tompkins, F.C. Classification and theory of solid reactions. In *Chemistry of the Solid State*; Academic Press: New York, NY, USA, 1955.
64. Kyaw, K.; Kubota, M.; Watanabe, F.; Matsuda, H.; Hasatani, M. Study of carbonation of CaO for high temperature thermal energy storage. *J. Chem. Eng. Jpn.* **1998**, *31*, 281–284. [[CrossRef](#)]
65. Schaube, F.; Koch, L.; Wörner, A.; Müller-Steinhagen, H. A thermodynamic and kinetic study of the de- and rehydration of $\text{Ca}(\text{OH})_2$ at high H_2O partial pressures for thermo-chemical heat storage. *Thermochim. Acta* **2012**, *538*, 9–20. [[CrossRef](#)]
66. Zhu, Y.; Mimura, K.; Isshiki, M. Oxidation mechanism of Cu_2O to CuO at 600–1050 °C. *Oxid. Met.* **2004**, *62*, 207–222. [[CrossRef](#)]
67. Prisedsky, V.V.; Vinogradov, V.M. Fragmentation of diffusion zone in high-temperature oxidation of copper. *J. Solid State Chem.* **2004**, *177*, 4258–4268. [[CrossRef](#)]

